N. I. Elkalashy, M. Lehtonen, H. A. Darwish, M. A. Izzularab and A.-M. I. Taalab, Modeling and Experimental Verification of High Impedance Arcing Fault in Medium Voltage Networks, IEEE Transactions on Dielectrics and Electrical Insulation, vol. 14, no. 2, pp. 375-383, April 2007.

Modeling and Experimental Verification of High Impedance Arcing Fault in Medium Voltage Networks

Nagy I. Elkalashy, Matti Lehtonen
Power Systems & High Voltage Engineering, Helsinki University of Technology (TKK)
Otakaari 5 I, Otaniemi, Espoo, PO Box 3000, FI-02015 HUT, Finland

Hatem A. Darwish, Mohamed A. Izzularab and **Abdel-Maksoud I. Taalab**
Electrical Engineering Department, Faculty of Engineering, Minoufiya Unversity, Shebin El-Kom, 32511, Egypt

ABSTRACT

A high impedance arcing fault due to a leaning tree in medium voltage (MV) networks is modeled and experimentally verified. The fault is represented in two parts; an arc model and a high resistance. The arc is generated by a leaning tree towards the network conductor and the tree resistance limits the fault current. The arcing element is dynamically simulated using thermal equations. The arc model parameters and resistance values are determined using the experimental results. The fault behavior is simulated by the ATP/EMTP program, in which the arc model is realized using the universal arc representation. The experimental results have validated the system transient model. Discrete Wavelet Transform is used to extract the fault features and therefore localize the fault events. It is found that arc reignitions enhance fault detection when Discrete Wavelet Transform is utilized.

Index Terms - **Arc simulation, ATP/EMTP, dynamic arc equations, high impedance arcing faults, faults due to leaning trees.**

1 INTRODUCTION

HIGH impedance faults often draw small currents which cannot be detected by conventional relays. When these faults persist, it is hazardous for both human beings and electrical equipment, especially when they are associated with arcs. Such faults are very common in distribution networks [1]. So, many protection algorithms have been introduced to detect these faults [1-7].

In the Nordic countries, fault categories are classified into snow burden 35%, fallen trees 27%, boughs on pole transformers 9%, diggers 6%, lightning impulses 6%, and the rest are probably caused by animals. Due to the forest area, the electrical network is exposed to faults due to leaning trees [2]. This fault is categorized as high impedance due to high resistance of the tree.

Recently, recorded field data have been used to enhance protection relay performance [2-4]. These data are used for practical investigation of network abnormal conditions or to test the relay reliability and its security. However, they are not suitable for modeling faults, especially high impedance faults. That is due to the fact that the fault characteristics cannot be managed using measurements at the network terminals. Furthermore, the fault scenario is not well-known and such data do not provide a dependable basis on which to base protection functions.

Consequently, many researchers have performed actual fault events on real networks and have captured fault data from ultimately known events and locations [4-7]. It is worthwhile to introduce practical protection functions using such data, especially if the fault event is recorded at both the fault branch and the measuring terminals. However, it imposes a high and severe risk on the electrical networks and there are restrictions against further use of staged faults. On the other hand, experimental work is still used to determine characteristics of the high impedance faults associated with arcs [8]. However, these investigations are insufficient for managing situations where several faults simultaneously occur at a number of locations in the network.

In order to overcome the complications of obtaining staged fault data or of studying difficult abnormal conditions in the electrical networks, accurate fault modeling incorporated in the networks at different locations reproduces the well-known fault circumstances. Avalanche data can also be used to introduce and examine relay functions. Fault modeling requires experimental data to fulfill its equations and their parameters. So in this paper, an experimental setup is used to establish a high impedance fault of a leaning tree type. The test results are used to model the fault. The model parameters are determined. The experimental work is implemented using the ATP/EMTP package. The tree impedance is represented using a resistance and the arc element is modeled by a thermal model and realized using universal arc representation in the ATP code. The simulation results are compared with the experimental results to examine the validity of the fault model. Then, fault signals are analyzed using Discrete Wavelet Transform (DWT) and its detection is also discussed using terminal data of a simulated 20 kV unearthed network.

Manuscript received on 22 June 2006, in final form 8 November 2006.

2 EXPERIMENTAL WORK

2.1 LABORATORY SET UP

An experiment has been performed to measure the characteristics of a high impedance fault occurring in a 20 kV distribution network. It was carried out at the Power Systems and High Voltage Laboratory, Helsinki University of Technology (TKK), Finland. Figure 1 shows the experimental configuration and corresponding parameters are indicated in Appendix 7.1. When the conductor is energized at 11.5 kV and the tree bends close, an arc is created as shown in Figure 2.

2.2 EXPERIMENTAL RESULTS

The experiment was accomplished in two steps. First, the tree resistance was measured when the tree and conductor were touching. The applied voltage on the tree was then increased gradually. At each increasing voltage step, the tree voltage and current values were measured to estimate the tree resistance as shown in Figure 3. The solid line was obtained using measured data, while the dotted one gives the data fitting that represents the initial resistance value. It is found equal to 201 kΩ. The dispersion of the experimental data can be much better estimated using the standard deviation. It represents the average variation as a function of the resistance value 201 kΩ and it is equal to 18 kΩ. The resistance value is related to the measuring location across the tree and the laboratory atmospheric conditions. However, when the temperature is less than -15 ^{o}C, the resistance is found to be approximately 800 kΩ for the same tree. Therefore, the tree resistance varies according to the annual season in the range of several hundreds of kΩ [3].

In the second step of the experiment, the fault characteristics were measured as described in the following scenario. The system voltage was applied to the conductor. As the tree was moved towards the conductor, however, the measured current was almost zero. When the tree was very close to the conductor bar, less than 2-3 cm, an arc was established initiating the current and distorting the voltage wave. The arc was then elongated by moving the tree away, to a distance greater than 4-7 cm, and hence the arc was extinguished. This scenario means the fault is "self-extinguishing", however, if the tree does not move far away from the conductor, the fault becomes permanent. Figure 4 illustrates the fault voltage and current waveforms when it is associated with arcs at different locations. It reveals that the distortions in voltage and current waveforms are influenced by the arc behavior. Therefore, non-steady state periods with spikes in the voltage and current waveforms have been evident at the reigniting instants. This is clearly depicted in the enlarged figures at the vicinity of the zero-crossings as shown in Figure 4a. Identification of these features can enhance this fault detection. On the other hand, if the arc is continuous the waveform pattern of voltage and current is as in Figures 4b and 4c.

3 ARC MODELING

It is extremely difficult to accurately simulate a complete arc circumstance due to its irregularity. The arc behavior changes from one half-cycle (power frequency) to the other as revealed by the experimental arc characteristics shown in Figure 5. This constitutes one cycle specific to an arc and it is characterized by unsymmetrical half-cycles. So, the arc model parameters extracted using the positive half-cycle are inappropriate for the others.

There are several models used for describing the arcs. Most models are used for circuit breaker arcs [9-10] and several of them have been applied to long arcs or arcing faults [11-12]. There are various concepts for arc modeling. The most popular rules depend on thermal equilibrium. The thermal model has the longest history of the dynamic arc models, since Cassie [13] and Mayr [14] introduced the first description of arc conductivity in the form of a first order differential equation. These dynamic equations have been improved and modified to increase the models' validity and reduce the computational burden. Also, they have been adapted to long arc representation as [11]:

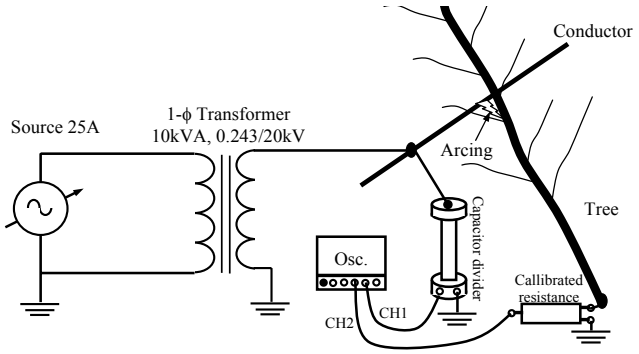

Figure **1.** Experimental configuration.

Figure 2. Arc-associated tree bending over the conductor.

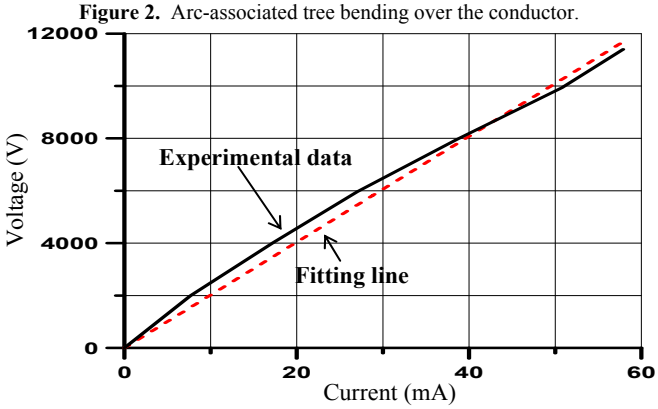

Figure 3. Tree resistance at laboratory atmospheric conditions.

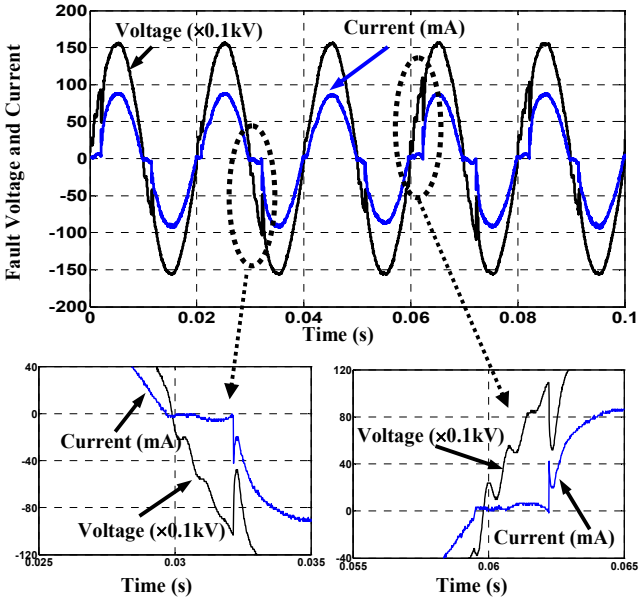

(a) Enlarged view of waveforms and zero-crossings when the fault is in the foliage.

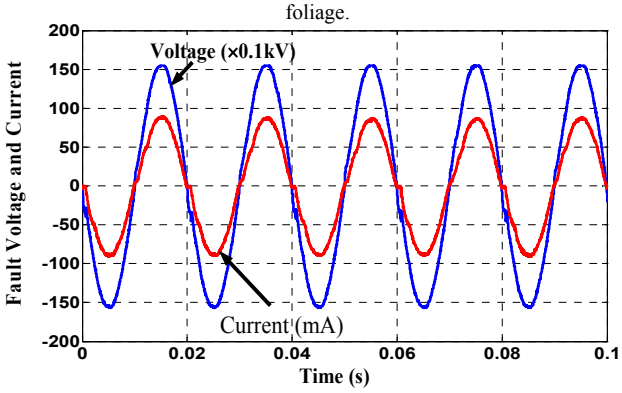

(b) The waveforms when the fault is at the branch.

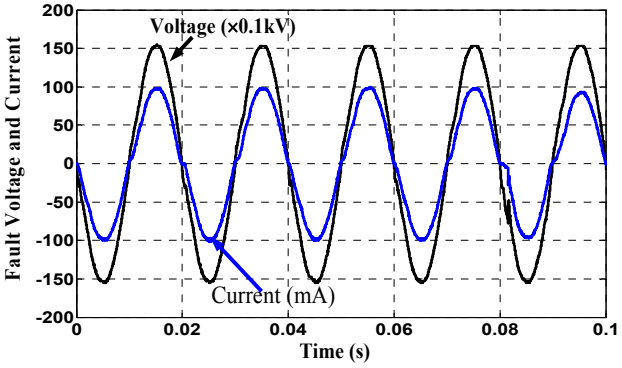

(c) The waveforms when the fault is at the trunk.

Figure 4. Experimental waveforms at different fault locations

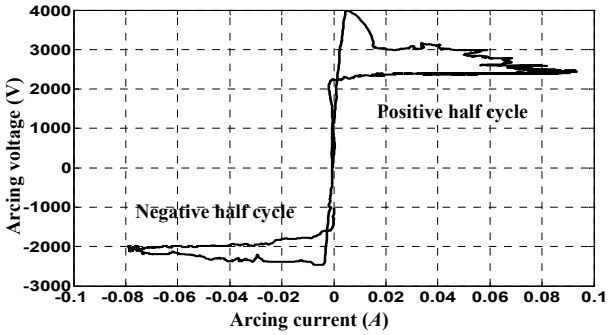

Figure 5. Experimental arc characteristics.

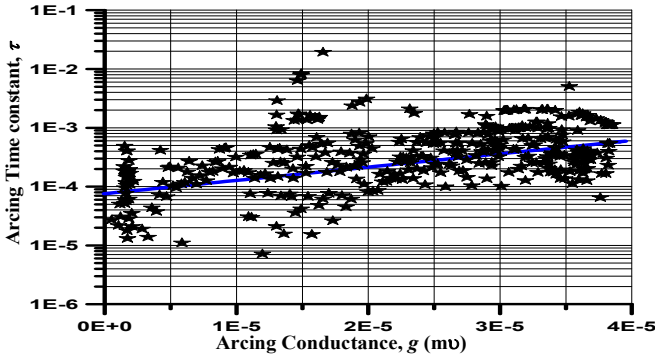

Figure 6. Arc time constant for the positive cycle.

$$\frac{dg}{dt} = \frac{1}{\tau}(G - g) \qquad (1)$$

where g is the time varying arc conductance, $G=|i|/V_{arc}$ is the stationary arc conductance, $|i|$ is the absolute value of the arc current, V_{arc} is a constant arc voltage parameter, and τ is the arc time constant. The equation parameters are determined so as to match the results from high arc current experiments. For arc representation associated with short arc length and small currents, they are changed to fit the new application.

To enable measurement of the arc characteristics, the arc position is experimentally moved to a new point between the tree and the calibrated series resistance. Therefore, the capacitor divider can then be connected across the arc element. The experimental characteristics shown in Figure 5 are used to determine the parameters of the arc equation (1). There are two unknown parameters needed in our application, V_{arc} and τ, of which V_{arc} describes the arc voltage clipping level. It can be determined when $dg/dt=0$, synchronized with the instant at which the maximum current occurs [11]. For the positive cycle it is found that V_{arc}=2520V. For determining τ, the arc equation is discretely written as:

$$\frac{g(k+1)-g(k)}{\Delta t} = \frac{1}{\tau}\left(\frac{|i(k)|}{V_{arc}} - g(k)\right) \quad k = 1,2,... \qquad (2)$$

Equation (2) contains the unknown parameter τ. Using the experimental data of the arc current and voltage, it can be determined as a function of arc conductance as shown in Figure 6. Consequently, τ is defined as:

$$\tau = Ae^{Bg} \qquad (3)$$

where A and B are constants. Using two fitting coefficients accurately tracks the arc nature. The arc hysteresis in the simulation phase is sensitive to τ, whose behavior during the half cycle is dominated by the constant B as evident from Figure 6. The suitable values are found to be A=6.6E-5 and B=41977 for the time constant shown in Figure 6. Figure 7 compares the simulated with the experimental arc characteristics. These results are obtained using the simulated system described in the following subsection. Although there is good agreement in the characteristics during the positive half cycle, the bad matching through the negative half cycle is obvious. On the other hand, the appropriate parameters for the negative half cycle shown in Figure 5 are V_{arc}=2100 V, A=2.0E-5, and B=85970.30. The corresponding simulated arc characteristic is illustrated in the comparison shown in Figure 8. These comparisons confirm the model accuracy.

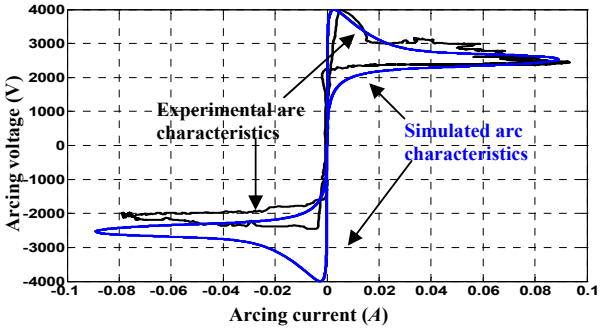

Figure 7. Comparison of simulated with experimental arc characteristics when fitting coefficients are used for positive half cycle data.

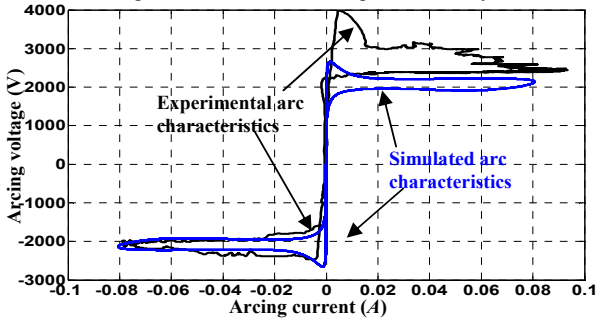

Figure 8. Comparison of simulated with experimental arc characteristics when fitting coefficients are used for negative half cycle data.

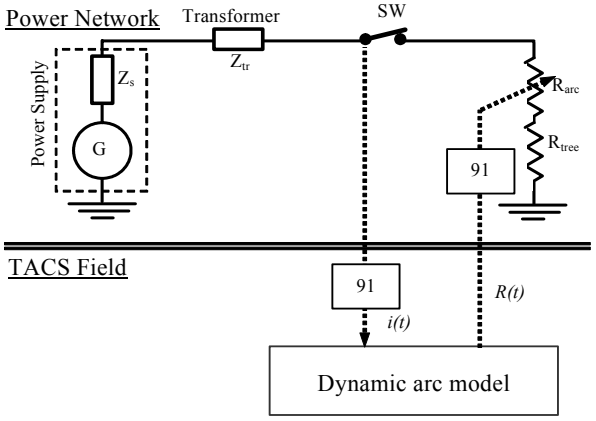

Figure 9. ATP/EMTP network used for modeling the fault.

4 SIMULATION RESULTS

The experimental system shown in Figure 1 has been implemented using the ATP/EMTP program as described in Appendix 7.2 with the parameters summarized in Appendix 7.1. Figure 9 illustrates the simulation circuit using the ATP/EMTP program. This circuit was realized using ATPDraw which is a graphical interface used to simplify the ATP/EMTP processing [15]. The arc model was implemented using the universal arc representation [16], in which the dynamic arc equation (1) is solved as illustrated in Appendix 7.2.

The control signal required for the controlled integrator and acquired from the case depicted in Figure 4a is shown in Figure 10a. Considering the conductance at the zero crossing associated with arc extinction, the dielectric of the medium until the instant of reignition is represented by a variable resistance as a ramp function of 0.5 MΩ/*ms* for a period of 1 *ms* after each zero-crossing and then 4 MΩ/*ms* until the reignition instant. These variables are used for matching the experimental current and voltage waveforms until the reignitions. They are compromise ramp values obtained with the aid of fitting the resistance curves computed from the experimental voltage and current during such periods. The corresponding simulated fault waveforms are illustrated in Figure 10b. In the same manner, the test case shown in Figure 4c has been simulated as shown in Figure 10c. The utilized fault parameters have been selected to be suitable for each case where the parameters R_{tree}, V_{arc}, A and B are found to be 140.5 kΩ, 2520 V, 5.6E-7 and 395917 for the first simulated case, and 130.0 kΩ, 2050 V, 8.5E-5 and 99987 for the other, respectively.

In the two simulated fault cases, the parameters A and B are compromised values for the positive and negative half cycles. In these cases, there are differences in the arc behavior. The first case is when the fault is in the foliage and there are frequent and obvious reignitions. However, the second case is when the fault is at the tree trunk and the impact of the arc in the form arc reignitions is reduced. Due to the differences in the arc behavior, the arc model parameters of each case are not the same as depicted in the aforementioned parameters. By comparing the simulated and experimental waveforms, it appears that the fault modeling due to a leaning tree is accurately represented.

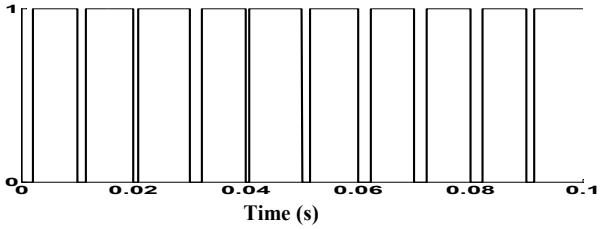

(a) Control signal to distinguish dielectric and arcing periods.

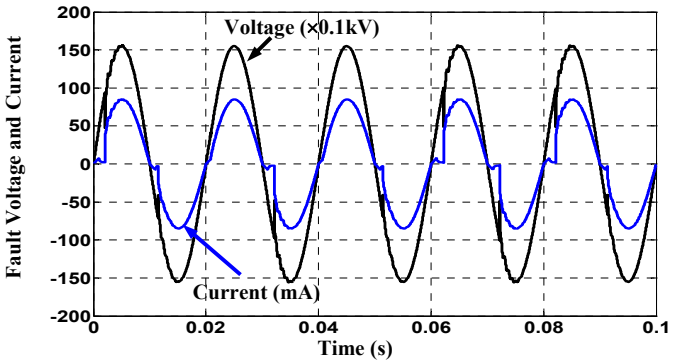

(b) Simulated waveforms of the case shown in Figure 4a.

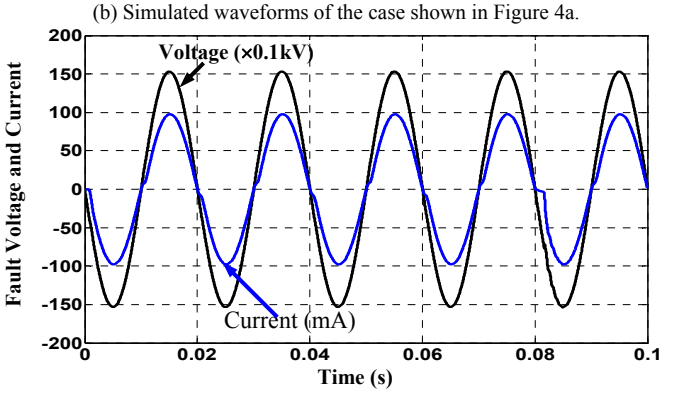

(c) Simulated waveforms of the case shown in Figure 4c.

Figure 10. Simulation results.

5 DWT-BASED FAULT FEATURES EXTRACTION

Due to the arc reignitions after each zero-crossing, the waveforms are not stationary. So, the Fast Fourier Transform (FFT) is not suitable for well-timed tracking because the arc is haphazard. It is important to use an appropriate signal processing technique such as Wavelet Transform.

Wavelets are families of functions generated from one single function, called the mother wavelet, by means of scaling and translating operations. They are oscillatory, decay quickly to zero, and integrate to zero. The scaling operation is used to dilate and compress the mother wavelet to obtain the respective high and low frequency information of the function to be analyzed. Then the translation is used to obtain the time information. In this way a family of scaled (dilated) and translated (shifted) wavelets is created and serves as the base for representing the function to be analyzed [17].

The discrete wavelet transform is in the form [17]:

$$DWT_{\psi} f(m,k) = \frac{1}{\sqrt{a_o^m}} \sum_n x(n) \psi\left(\frac{k - n b_o a_o^m}{a_o^m}\right) \quad (4)$$

where $\psi(.)$ is the mother wavelet that is discretely dilated by the scale parameter $a^m{}_o$ and translated using the translation parameter $nb_o a^m{}_o$, where a_o and b_o are fixed values with $a_o>1$ and $b_o>0$. m and n are integers. In the case of the dyadic transform, which can be viewed as a special kind of DWT spectral analyzer, $a_o=2$ and $b_o=1$. DWT is implemented using a multistage filter with down sampling of the low-pass filter output.

5.1 COMPARISON OF THE FAULT FEATURES

Several wavelet families have been tested to extract the fault features using the Wavelet toolbox incorporated into the MATLAB program [18]. The details d1 and d2 are not considered in order to avoid the experimental noise effect [19]. There is a strong relation between the mother wavelet, sampling frequency and frequency range that is required to be extracted. These experimental data are acquired at sampling rate equal to 100 kHz and it is considered for the feature extraction process. It is found that Daubechies wavelet 14 (db14) is appropriate to localize this fault. Details d3 and d4 including the frequency bands 12.5-6.125 and 6.25-3.125 kHz are highlighted. Features of the experimental case depicted in Figure 4a and its simulation are analyzed. The corresponding details d3 and d4 are shown in Figures 11 and 12, respectively. Comparing the details shown in Figure 11 with Figure 12 illustrates that the behavior of DWT is better when the experimental waveforms are used than with the simulated ones. That is because the arc extinction after the zero crossing is simulated using a linear high ramp resistance. However, it reveals that the details can localize the instant of arc reignitions. So, DWT can be used to extract this fault features.

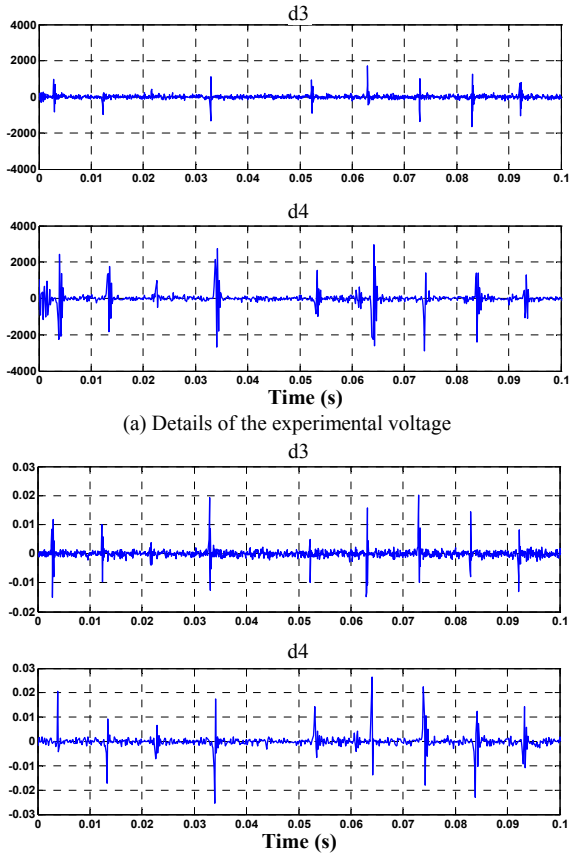

(a) Details of the experimental voltage

(a) Details of the experimental current

Figure 11. Details of the experimental case shown in Figure 4a.

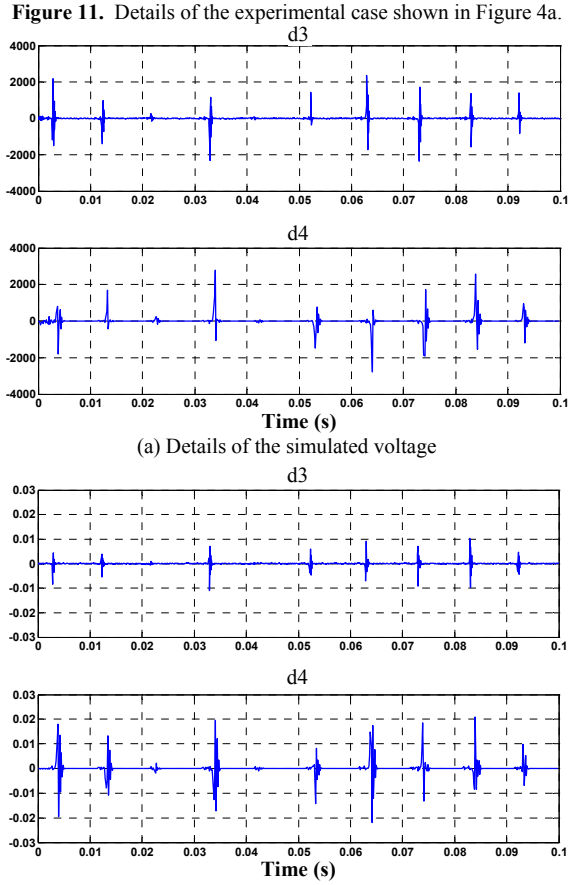

(a) Details of the simulated voltage

(b) Details of the simulated current

Figure 12. Details of the simulated waveforms shown in Figure 10b.

The main obstacle of this fault identification is that its features overlap other faults and furthermore, they may be dissipated when the signals are measured at substations because the fault current is very small. However, the fault can be recognized by considering these fingerprints on the residual current and voltage waveforms. Therefore, it is important to implement the fault at different locations in the network and to test a capability of this fault detection as following discussed.

5.2 FAULT DETECTION

Figure 13 is a single line diagram of a 20 kV unearthed distribution network simulated using ATP/EMTP and preprocessed by ATPDraw, as is depicted in Appendix 7.3. The line frequency dependent model in EMTP is intentionally selected to account for unsymmetrical faults. When the network and the fault modeling are combined in one arrangement, the network behavior during this fault can be investigated.

In Nordic Countries, the neutral is commonly unearthed and compensated MV networks are increasingly being used [20]. In this study, the neutral of the main transformer is isolated consistent with an unearthed system. Although this network is not intentionally connected to the earth, it is grounded by the natural phase to ground capacitances. Therefore, the fault phase current is very low allowing a high continuity of service. The current distributions in unearthed networks during ground faults are discussed in [20].

The earth fault protection can be based on residual voltage and current. Their waveforms are digitally computed as:

$$u_r = u_a + u_b + u_c \quad (5)$$

$$i_r = i_a + i_b + i_c \quad (6)$$

where u_r and i_r are the residual voltages and currents, respectively. u_a , u_b and u_c are the phase voltages. i_a , i_b and i_c are the phase currents. Figure 14 illustrates the residual voltage and current waveforms at the measuring point as illustrated in Figure 13. The fault parameters of the experimental case depicted in Figure 4a are used for implementing the fault event when it is started at 0.026 s. The corresponding residual current is very small and the impact of the initial transients (charges/discharges) due to the arc reignitions is obvious after each zero-crossing. These transients are traveled and attenuated for approximately one-quarter of the power cycles, as illustrated in the enlarged view of the residual current shown in Figure 14b. Even though the initial transients are due to the arc reignitions, they are controlled not only by the fault characteristics but also by the electrical network parameters, fault location and fault instant.

Figure 15 illustrates the waveforms when the fault location is changed along the faulty feeder L1 to a fault distance L_f equal to 5 km. It reveals that the waveform magnitudes are not changed by altering the fault location because the fault is a high impedance type. However, the initial transients due to arc reignitions are changed, as shown in the enlarged view, and they are also changed if the fault instant is altered.

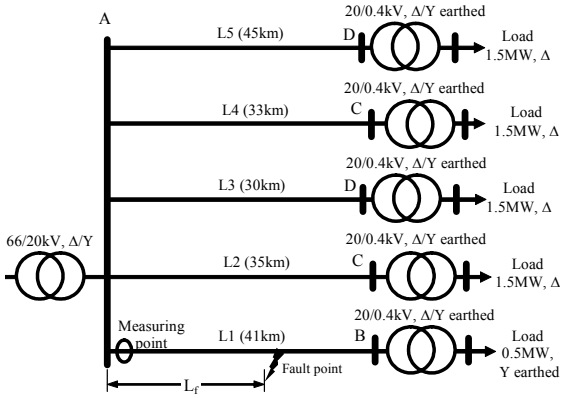

Figure 13. Simulated system

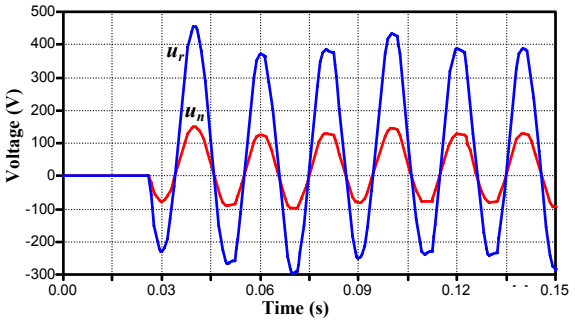

(a) Neutral and Residual voltages (u_n and u_r, respectively).

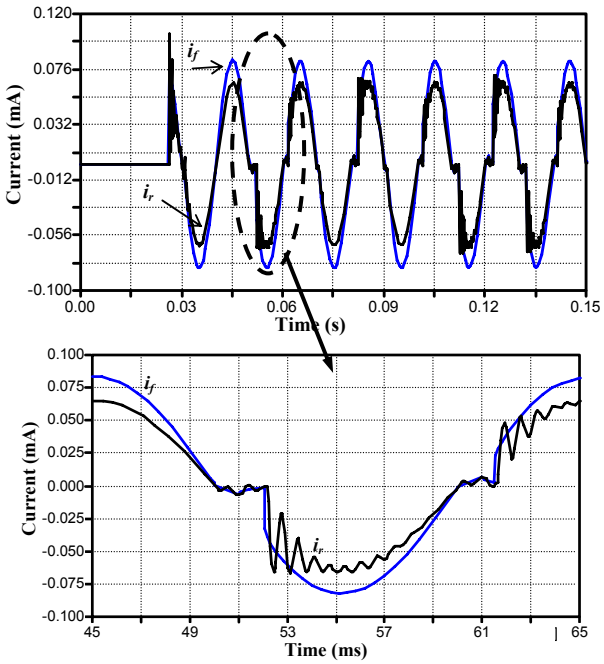

(b) Enlarged view of residual current waveforms (i_r)

Figure 14. The transient waveforms when the fault occurs at the end of feeder L1 on the unearthed network.

The Daubechies wavelet 14 (db14) is also used to extract features of the fault case shown in Figure 14, in which the sampling frequency of 100 kHz is considered. However, DWT execution time is one of limitation issues restricting its practical implementation. This issue is in the phase of overcoming where DWT has been experimentally implemented using DSP board with reducing its lengthy execution time as discussed in [19]. The sampling rate can be reduced; however, a different mother wavelet should then be

used. The corresponding details are shown in Figure 16. It is obvious that the responses of the DWT to initial transients frequently appear with each zero crossing due to the arc reignitions. This confirms that the fault features are highlighted not only at starting instants of the fault events but also during the fault period. So, the periodicity of arc reignitions is a significant behavioral trait associated with faults due to a leaning tree. Therefore, the DWT performance ensures the fault detection.

It is obvious that this fault impact on the network is very small. However, distributed wireless sensors are recently installed at different locations in the electrical networks. They are sensitive to the small change in the network. Moreover, the electrical quantities can be gathered from different locations in the network and therefore the protection function can be applied on a wide range for the electrical network measurements. This will be considered in a future work.

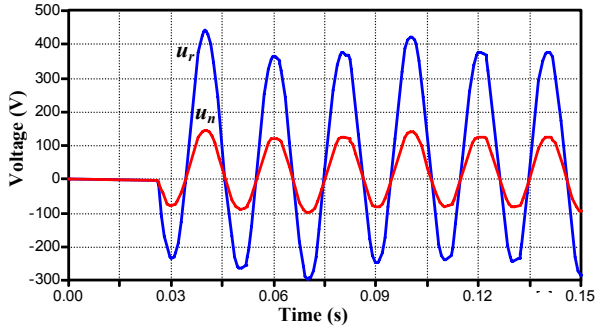

(a) Neutral and residual voltages (u_n and u_r, respectively).

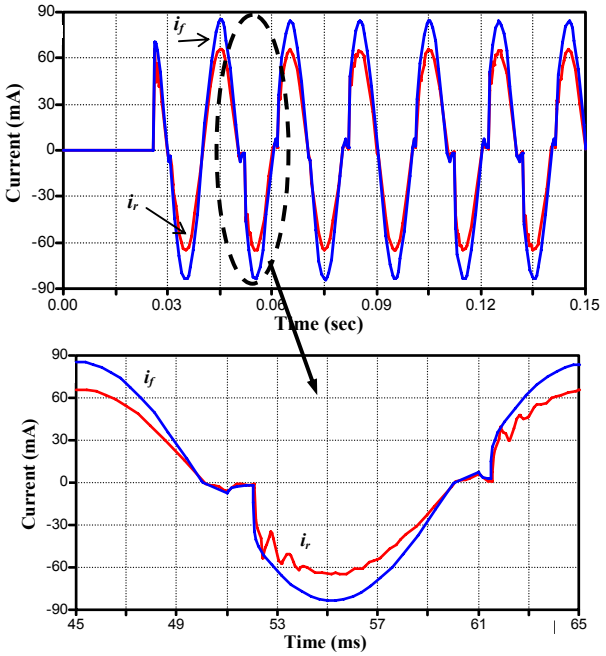

(b) Enlarged view of fault and residual currents (i_f and i_r).

Figure 15. The transient waveforms when L_f is equal to 5 km.

6 CONCLUSIONS

High impedance faults due to a leaning tree have been investigated and the arc associated with the corresponding small fault current has been accurately modeled. An experiment was carried out to ascertain the fault features and therefore aid their simulation. The arc model parameters were estimated using the dynamic arc equation and the complete circumstances of the experimental test cases were simulated. The fault modeling has been incorporated in a 20 kV unearthed network. Analysis using DWT has been carried out and the results prove the fault detection method. The DWT has a specific performance with this fault type, in which the periodicity of the arc reignitions enhances the fault identification. So, sensitive and secure detection of the faults due to a leaning tree can be carried out based on DWT and this will be extended in work to follow. In this work, this fault detection and location will be discussed considering the current measurements at different locations in the network.

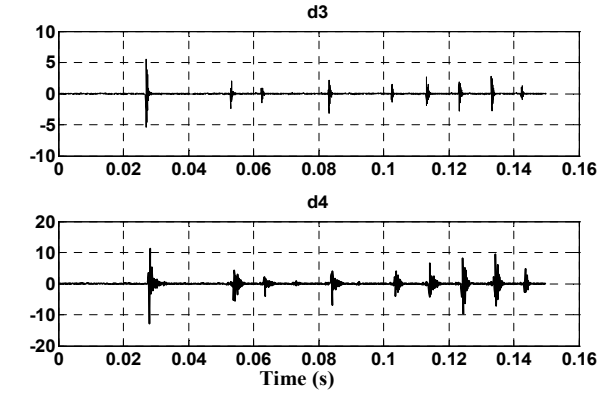

(a) Details of the residual voltage waveform.

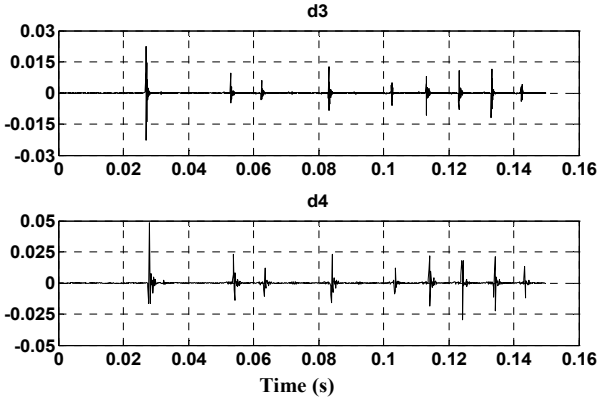

(b) Details of the residual current waveform.

Figure 16. Details of the fault case shown in Figure14.

7 APPENDIX

7.1 EXPERIMENTAL SET UP DATA

With the aid of the experimental configuration shown in Figure 1, the capacitor divider and calibrated resistance are used for transforming the fault voltage and current signals respectively to be suitable inputs to the oscilloscope. The experimental setup data are:

Source:	25 A, 50 Hz, 2.6% short circuit impedance (using transformer bases).
Transformer:	10 kVA, 0.243/20 kV, 4.2%
Calibrated resistance:	0.490488 Ω.
Capacitor divider:	High voltage 100 PF, 100 kV, Low voltage 100 nF with calibrated scale factor 994.
Oscilloscope and PC.	
Atmospheric conditions:	T=20 °C, PH%=12.8 and P=1016.15 hPa.

7.2 UNIVERSAL ARC REPRESENTATION USING ATPDRAW

Referring to the dynamic arc equation (1), the arc current is inputted into the Transient Analysis Control Systems (TACS) field as shown in Figure 17. Its absolute value is divided by the constant arc voltage parameter V_{arc} and then the outcome minus the arc conductance computed in the previous step is divided by the arc time constant τ as described in equation (3). The resultant is inputted to the Controlled Integrator type 58 to solve equation (1). So, the arc conductance is updated at each time step. Its inverse value is passed back to the power network using TACS controlled resistance type 91 and so on. Therefore, the arc interaction with the electrical power network is accomplished. However, the integrator output is equal to the reset signal RES when the control signal CTR is low. This option is valuable for representing reignition events after current zero crossing as depicted in Figure 4a. When the control signal is high, the dynamic arc equation is solved as mentioned but when it is low, the reset value RES dominates in forming the dielectric withstand against recovery voltages. The corresponding ATPDraw network is shown in Figure 18.

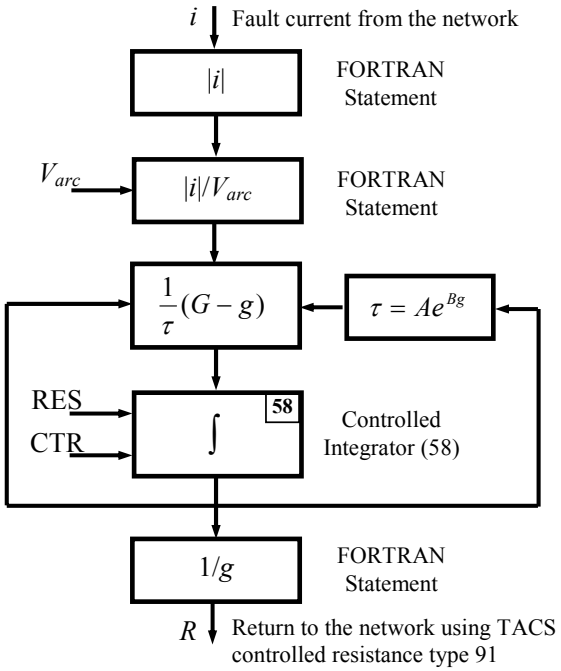

Figure 17. Universal arc representation of the associated arc.

7.3 SIMULATED SYSTEM

Figure 19 illustrates the ATPDraw network under consideration. It contains the MV network described in Figure 13, the universal arc representation and the residual voltage and current (u_r and i_r) equations (5) and (6), respectively. The line is represented using the frequency dependent JMarti model according to the configuration shown in Figure 20.

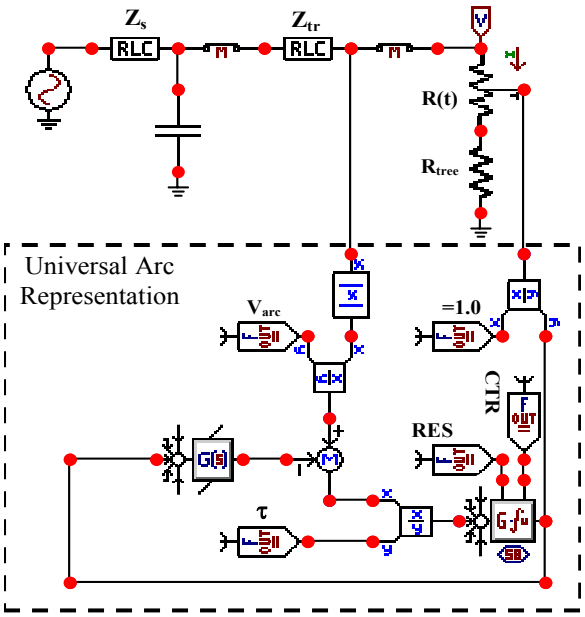

Figure 18. The ATPDraw network of the experimental setup.

8 ACKNOWLEDGMENT

The authors gratefully acknowledge the assistance with experimental measurements of Mr. Hannu Kokkola and the discussions with Mr. John Millar.

9 REFERENCES

[1] Report of Power System Relaying Committee (PSRC) Working Group D15, “High Impedance Fault Detection Technology”, 1996.

[2] S. Hanninen, M. Lehtonen and T. Hakola "Earth Faults and Related Disturbances in Distribution Networks", Proc. IEEE/PES SM2001, Vancouver, Canada, 2001.

[3] S. Hanninen and M. Lehtonen, "Method for Detection and Location of Very High Resistive Earth Faults", Europ. Trans. Electr. Power, ETEP, Vol. 9, pp. 285-291, 1999.

[4] B. D. Russell and C. Benner, "Arcing Fault Detection for Distribution Feeders: Security Assessment in Long Term Field Trials", IEEE Trans. Power delivery, Vol. 10, pp. 676-683, 1995.

[5] G. Benner and B. Russell, "Practical High Impedance Fault Detection on Distribution Feeders", IEEE Trans. Ind. Appl., Vol. 33, pp.635-640, 1997.

[6] A. Sultan, G. Swift and D. Fedirchuk "Detecting Arcing Downed-Wires Using Fault Current Flicker and Half-Cycle Asymmetry", IEEE Trans. Power delivery, Vol. 9, pp. 461-470, 1994.

[7] L. Prikler, M. Kizilcay, G. Ban and P. Handl, "Improved Secondary Arc Models Based on Identification of Arc Parameters from Staged Fault Test Records", 14th Power System Computation Conference (PSCC), Sevilla, 2002.

[8] A. Sedighi, M. Haghifam, O. Malik and M. Ghassemian, "High Impedance Fault Detection Based on Wavelet Transform and Statistical Pattern Recognition", IEEE Trans. Power delivery, Vol. 20, pp. 1414-2421, 2005.

[9] CIGRE WORKING GROUP 13.01 ”Applications of Black Box Modeling to Circuit Breakers” Electra, no. 149, 1993.

[10] P. Schavemaker and L. Sluis, “An Improved Mayr-Type Arc Model Based on Current-Zero Measurements”, IEEE Trans. Power delivery, Vol. 15, pp.580-584, 2000.

[11] M. Kizilcay and T. Pniok, “Digital Simulation of Fault Arcs in Power systems”, Europe Trans. Electr. Power Syst., ETEP, Vol. 4, pp. 55-59, 1991.

[12] V. Terzija and H. Koglin, “Long Arc in Free Air: Laboratory Testing, Modeling, Simulation and Model Parameters Estimation”, IEE Proc. Gener. Transm. Distrib., Vol. 49, pp. 319-325, 2002.

[13] A. M. Cassie, Theorie Nouvelle des Arcs de Rupture et de la Rigidit\é des Circuits: Cigre, Report 102, pp. 588-608, 1939.

[14] O. Mayr, “Beitrage zur Theorie des Statischen und des Dynamischen Lichthogens,” Archiv f\ür Elektrotechnik, vol. Band 37, no. Heft 12, pp. 588-608, 1943.

[15] L. Prikler and H. Hoildalen, *ATPDraw Users Manual*, SINTEF TR A4790, 1998.

[16] H. Darwish and N. Elkalashy "Universal Arc Representation Using EMTP", IEEE Trans. Power Delivery, Vol. 2, pp 774-779, 2005.
[17] M. Solanki, Y. Song, S. Potts and A. Perks, "Transient protection of transmission line using wavelet transform", 7th Intern. Conf. Developments in Power System Protection, (IEE), pp. 299–302, 2001.
[18] *Wavelet Toolbox for MATLAB*, Math Works, 2005.
[19] H. A. Darwish, M. H. Farouk, A. I. Taalab and N. M. Mansour "Investigation of Real–Time Implementation of DSP-Based DWT for Power System Protection", IEEE PES Transmission and Distribution Conf. Exposition, Dallas, Texas, USA, 2006.
[20] M. Lehtonen and T. Hakola "Neutral Earthing and Power System Protection. Earthing Solutions and Protective Relaying in Medium Voltage Distribution Networks", ABB Transmit Oy, FIN-65101 Vassa, Finland, 1996.

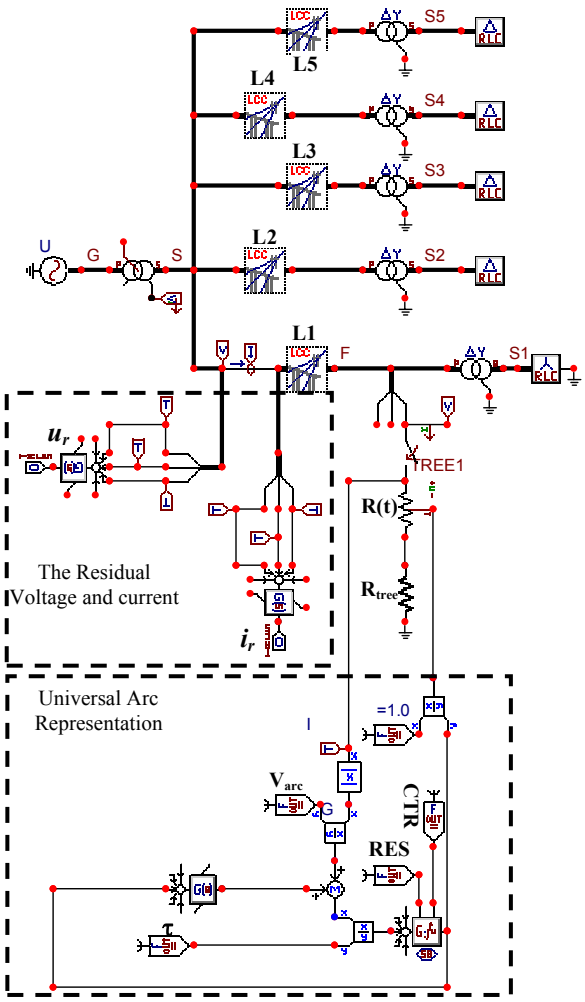

Figure 19. The ATPDraw network of the simulated system.

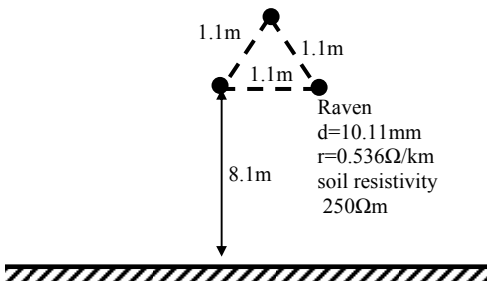

Figure 20. The transmission line configuration.

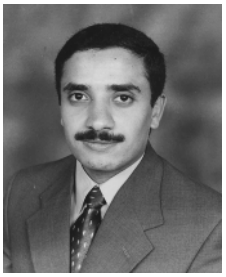

Nagy I. Elkalashy (S'06) was born in Quesna, Egypt on 4 August 1974. He received the B.Sc. (first class honors) and M.Sc degrees from the Electrical Engineering Department, Faculty of Engineering, Shebin El-Kom, Menoufiya University in 1997 and 2002, respectively. Currently, he is working towards the Ph.D. degree at Power Systems and High Voltage Engineering, Helsinki University of Technology (TKK), Finland under joint supervision with Menoufiya University. His research interests are high impedance fault detection, power system transient studies including AI, EMTP simulation, and switchgear.

Matti Lehtonen (1959) was with VTT En-ergy, Espoo, Finland from 1987 to 2003, and since 1999 has been a professor at the Helsinki University of Technology, where he is now head of Power Systems and High Voltage Engineering. Matti Lehtonen received both his Master's and Licentiate degrees in Electrical Engineering from Helsinki University of Technology, in 1984 and 1989 respectively, and the Doctor of Technology degree from Tampere University of Technology in 1992. The main activities of Dr. Lehtonen include power system planning and asset management, power system protection including earth fault problems, harmonic related issues and applications of information technology in distribution systems.

Hatem A. Darwish (M'06-SM'06) was born in Quesna, Egypt on 13 September 1966. He received the B.Sc. (honors), M.Sc., and Ph.D. degrees in electrical engineering from Menoufiya University, Egypt in 1988, 1992, and 1996; respectively. From 1994 to 1996, he was working toward the Ph.D. degree at Memorial University of Newfoundland (MUN), St. John's, Canada based on Joint Supervision with Menoufiya University. He has been involved in several pilot projects for the Egyptian industry for the design and implementation of numerical relays, SCADA, fault location in MV feeders, distribution management systems, protection training packages, and relay coordination. His interests are in digital protection, signal processing, system automation, and EMTP ac/dc simulation, and switchgear.

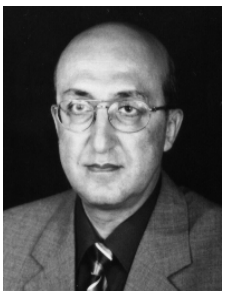

Mohamed A. Izzularab was born in Tanta, Egypt on 1950. He received the B.Sc. degree in electrical engineering from Menoufiya University, Egypt in 1973. He was awarded the M.Sc. degree from Elmansoura University in 1978 and Dr. Ing degree from I.N.P.T. Toulouse, France in 1983. Also he was awarded the D.Sc. in electrical engineering from Paul Sabatier University Toulouse, France in 1987. He obtained the Cigre Award for the best-applied research for the year 1998. Dr. Izzularab is the vice dean of the Faculty of Engineering, Menoufiya University.

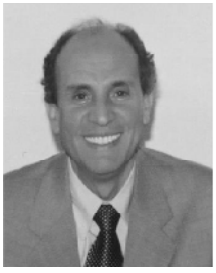

Abdel-Maksoud I. Taalab (M'99–SM'03) received the B.Sc. degree in 1969, in electrical–engineering from Menoufiya University, Egypt, the M.Sc. and Ph.D. degrees from Manchester University, U.K., in 1978, and 1982, respectively. In the same year of his graduation, he was appointed as an assistant professor at the Menoufiya University. He joined GEC Company in 1982. He is now a full Professor at the department of Electrical Engineering, Faculty of Engineering and vice dean of the Desert Environment Institute, Menoufiya University. His interests are in HVDC transmission systems, power system protection, and power electronics applications.